LUND UNIVERSITY

Department of Physics

LUP

Lund University Publications

On the dependence of the laser-induced incandescence (LII) signal on soot volume fraction for variations in particle size

Henrik Bladh[1], Jonathan Johnsson[2], Per-Erik Bengtsson[3]

    1 Division of Combustion Physics, Lund Institute of Technology,
        P.O. Box 118, SE-221 00 Lund, SWEDEN
        Telephone: +46 46 222 03 53
        Telefax: +46 46 222 45 42
        Mail: henrik.bladh@forbrf.lth.se (*Corresponding author*)
    2 Division of Combustion Physics, Lund Institute of Technology,
        P.O. Box 118, SE-221 00 Lund, SWEDEN
        Telephone: +46 46 222 47 56
        Telefax: +46 46 222 45 42
        Mail: jonathan.johnsson@forbrf.lth.se
    3 Division of Combustion Physics, Lund Institute of Technology,
        P.O. Box 118, SE-221 00 Lund, SWEDEN
        Telephone: +46 46 222 31 09
        Telefax: +46 46 222 45 42
        Mail: per-erik.bengtsson@forbrf.lth.se

Short title (max 120 characters): On the dependence of the laser-induced incandescence (LII) signal on soot volume fraction

Abstract

 "The laser-induced incandescence (LII) signal is proportional to soot volume fraction" is an often used statement in scientific papers, and it has – within experimental uncertainties – been validated in comparisons with other diagnostic techniques in several investigations. In 1984 it was shown theoretically in a paper by Melton that there is a deviation from this statement in that the presence of larger particles leads to some overestimation of soot volume fractions. In this paper we present a detailed theoretical investigation of how the soot particle size influences the relationship between LII signal and soot volume fraction for different experimental conditions. Several parameters have been varied; detection wavelength, time and delay of detection gate, ambient gas temperature and pressure, laser fluence, level of aggregation and spatial profile. Based on these results we are able, firstly, to understand how experimental conditions should be chosen in order to minimize the errors introduced when assuming a linear dependence between the signal and volume fraction and secondly, to obtain knowledge on how to use this information to obtain more accurate soot volume fraction data if the particle size is known.

1   Introduction

Laser-induced incandescence (LII) is a laser-based technique for particle measurements, which during the last decade has been frequently applied to flames and exhausts containing soot particles [1,2]. The detected LII signal is the thermal radiation from particles that have undergone rapid heat-up by a short laser pulse, often with duration on the order of 10 nanoseconds. Initially the particles are heated to high temperatures, often around 4000 K. The particles then cool down to the surrounding gas temperature by different heat loss processes, of which the heat conduction to the surrounding gas dominates shortly after the laser pulse. A common application of laser-induced incandescence (LII) is to measure soot volume fraction in flames and exhausts containing soot particles.

The soot volume fraction, f_v, can be simply expressed as the number concentration, N, of particles multiplied by the volume of each particle. For a monodisperse size distribution of spherical particles with diameter, D, the soot volume fraction can be expressed as

$$f_v = N \frac{\pi D^3}{6}. \tag{1}$$

The first study to explore the relationship between the LII signal and the soot volume fraction was made by Melton [3]. He made a theoretical study treating the heat and mass balance equations for laser-heated particles, and in the limit of high laser power and maximum particle temperature he arrived at an expression where the LII signal was found to be proportional to D^x, where

$$x = 3 + \frac{0.154}{\lambda_{\text{det}}} \tag{2}$$

and the detected wavelength, λ_{det}, is expressed in micrometers. For a detection wavelength of 700 nm $x = 3.22$, and for 400 nm $x = 3.38$. The study by Melton thus indicated that there is a deviation from a linear relationship between LII signal and soot volume fraction for variations in particle diameters and also that longer detection wavelengths are preferable from this point of view.

About a decade later, several investigations were made to experimentally explore the relationship between LII signal and soot volume fraction. Vander Wal and Weiland [4] performed experiments in premixed flat flames at a specific height for different equivalence ratios and compared LII signals with soot volume fractions calculated from extinction measurements. The LII signals showed good correlation with soot volume fractions within the experimental uncertainties also for higher equivalence ratios where the relative occurrence of larger soot particles is expected to be high. In a work by Bengtsson and Aldén [5], LII signals in premixed flat flames were measured as a function of height above the burner for a specific equivalence ratio. The LII signals were compared with soot volume fractions evaluated from extinction measurements. The agreement was relatively good but the LII signal curve was found to be steeper than the soot volume fraction curve evaluated from extinction data. Since the particle diameters show a strong increase versus height above burner in this type of flame [6], a steeper LII curve is in agreement with an exponent x higher than 3 in Eq. 2. Similar experiments where LII signals were compared with soot volume fractions evaluated from extinction measurements were made in diffusion flames at different flame heights by Santoro and co-workers [7-9], and it was found that the agreement between LII signals and soot volume fractions was generally good.

In one of these papers [9] it was, however, said that the small difference (~5-10%) between LII data and scattering/extinction data probably is due to a particle size effect since "the deviation usually occurs at lower heights or along the flame centre line where soot particles are smaller".

At the end of the 90's Seitzman and co-workers made several investigations on the relationship of LII signal to soot volume fraction [10-12]. LII data was compared with soot volume fractions calculated from extinction measurements in flames and observed differences led to the suggestion that particle size differences were the cause for the discrepancy. They made a theoretical investigation of how the soot volume fraction varied for changes in particle size for some different experimental conditions, and based on their results they concluded that a short prompt detection gate and a long detection wavelength is preferable for achieving linear relationship between LII signal and soot volume fraction. In the last of the aforementioned studies by the group of Seitzman [12], they produced artificial soot particles in a soot generator and made LII measurements for variations of carbon concentrations of four orders of magnitude. They studied the LII signal as a function of soot concentration for different soot particle size and found their data to scale as $D^{3.45}$, while their calculations scaled as $D^{3.41}$.

Nowadays it is often accepted that the LII signal is proportional to the soot volume fraction without considering that soot particle sizes may differ largely in the measurement volume, an approach that very well may introduce large uncertainties in the results. The problem can, however, be circumvented by using the 2-color LII technique (see for instance [13]). In this technique the soot volume fraction is derived using the particle temperature history from time-resolved pyrometry in addition to the LII signal intensity and not by only relating to the LII signal intensity itself. The 2-color LII technique is, however, only applicable to point measurements and laser fluences below the sublimation threshold and cannot be considered for imaging soot volume fraction for instance in internal combustion engines [14]. In such situations there simultaneously exist volumes where soot nucleation occurs, i.e. where the soot particles generally are small, as well as volumes with larger particles. If there is no available information about the soot particle sizes from additional measurements, spatial regions with small particles will lead to an underestimation of the soot volume fraction if the exponent x is larger than 3 according to the theoretical analysis by Melton. Scientific papers claiming this relationship refer now and then to the theoretical investigation by Melton and/or to experimental comparisons of LII data with soot volume fractions evaluated from scattering/extinction data. Since there is a lack of recent theoretical investigations on this topic, as pointed out in [2], and also because this relationship is a very central theme in LII research, we have in this study made a detailed theoretical analysis of the relationship between LII signal and soot volume fraction for our current LII model. In these calculations we have used various input parameters to simulate different experimental situations. The aim of this paper is thus 1) to study how different experimental conditions influence the dependence of LII signals on the soot volume fraction (where the sizes vary), 2) to learn how the experimental conditions should be chosen to minimize the size effect in this relationship, and 3) to gain knowledge on how to potentially compensate for this size dependence to improve quantitative soot volume fraction measurements.

2   Theory and methodology

The relationship between the signals obtained from laser-induced incandescence (LII) and the soot volume fraction is quite complex in nature and depends on many experimental and physical parameters. Data from such an analysis therefore tends to be complex, and a suitable selection and representation of the data will be of crucial importance in order to present a thorough and yet relevant picture for LII experimentalists. The intention of this section is to describe our methodology both for extracting the data, and for their representation.

Theoretical investigations with regards to the LII signal and soot volume fraction relationship must necessarily start with definitions of the two quantities under investigation. This would include the use of a theoretical model for predicting LII signal response under different conditions, and an appropriate model for the soot volume fraction in a gas. In this work certain general assumptions are made. Firstly, we assume that the primary particles are spherical, which means that Eq. 1 can be used to describe the soot volume fraction and that our current model for LII, which relies on spherical description of the primary particles, can be applied. Secondly it is assumed that the LII signal scales linearly with the particle number density N, thus signal absorption and laser attenuation effects are considered negligible. Since the soot volume fraction (Eq. 1) also scales linearly with N, the relationship between the LII signal and the soot volume fraction can be reduced to the relationship between the LII signal and the primary particle size for varying conditions.

The model for LII used in this work is described in detail in Appendix A followed by a nomenclature list in Appendix B, and only a brief description is given here. The model is based on a heat and mass balance for fractal aggregates of spherical soot particles when heated by laser radiation. The modelled physical processes are depicted in Fig. 1. The laser-induced incandescence signal, S_{LII}, can be written as [15,16]

$$ S_{\mathrm{LII}} \propto \pi D^2 N_p \int_0^\infty R(\lambda') \frac{4\pi D E(m)}{\lambda'} \frac{2\pi hc^2}{\lambda'^5} \left(\frac{1}{e^{hc/\lambda' k_B T} - 1} - \frac{1}{e^{hc/\lambda' k_B T_g} - 1} \right) d\lambda', \qquad (3) $$

using the Rayleigh-Debye-Gans theory for poly-fractal aggregates (RDG-PFA) which enables the emissivity of soot particles to be written according to the Rayleigh approximation, at least if the primary particles are sufficiently small (See App. A). Since the signal expression is explicitly dependent on D^3, the deviation from a pure linear relationship to soot volume fraction has its origin in the expression within brackets, which is a function of both detection wavelength and particle temperature. The particle temperature history during the LII process is dependent on all the terms in the heat and mass transfer equations, and these terms have different dependencies on the primary particle diameter. The absorption, radiation and internal energy processes are all assumed to be proportional to the particle volume ($\propto D^3$), whereas the heat conduction and sublimation processes are dependent on the area ($\propto D^2$) at low pressures with deviation to even weaker dependence for higher pressures due to the increased importance of the continuum regime terms (See App. A). Sublimation only occurs during and shortly after the laser pulse and therefore has to compete with the absorption making its influence less strong. At later times after the laser pulse, the dominating process is the heat conduction and the deviation from pure D^3-dependence is large, which is utilized when the LII technique is used for particle sizing. In Fig. 2 the modelled primary particle temperature is shown as function of time for two

particle sizes at high- and low-fluence conditions. The sizes have been chosen to represent the upper and lower limit of those typically encountered during LII measurements in sooting flames and only the size range defined by these limits will be investigated in this work. The results shown in Fig. 2 indicate that a size dependence of the particle temperature, and thus also of the expression within brackets in Eq. 3, exists at conditions typically encountered during soot volume fraction measurements in flames. We end this short discussion of the different dependencies by noting that the detection wavelength, which turns up in the expression by Melton (Eq. 2), only acts as a scaling factor on the temperature T in Eq. 3. The choice of detection wavelength will thus only be expected to show influence on the size dependence of the LII signal when a size dependence truly exists for the particle temperature.

The results presented in this paper will inevitably depend on the ability of the current LII model to predict the behaviour of the laser heating and cooling processes. In several studies models similar to the one used in this work have proved able to adequately describe the real case, but such investigations all rely on the final results produced by the model, like for instance the LII signal and, using 2-color LII, the particle temperature. The results presented in this work rely on the individual strength and size-dependence of the underlying terms, which is much more challenging to validate. This is especially the case for the sublimation term, which will be affecting the relationship between the signal and the volume fraction at higher fluences. Additional uncertainties are introduced by the fact that the model for LII to date has not been fully validated to all possible experimental conditions, like for instance at high laser fluence, low gas temperature and high level of aggregation. We still firmly believe that the results from the model will be able to decrease the uncertainties in evaluated soot volume fraction from LII signals and that the trends are representative for the real case. How well a compensation for the particle-size effect works may be investigated using well-controlled experiments where soot volume fractions are evaluated using both LII and an alternative technique.

The results from the investigations will be presented using two different approaches. The intention is partly to put the results in a historic context, and therefore the original results from Melton will be investigated in more detail. Since Melton's expression has the form of a power law, we have firstly chosen to present the LII signal to particle size relationship in a so called Duane plot [17], which is a log-log representation of the data. In such a representation a pure power law will result in a straight line with a slope corresponding to the exponent due to

$$y = c \cdot D^x \quad \Leftrightarrow \quad \log y = \log c + x \log D. \qquad (4)$$

where c is a constant. If time-integrated LII signals are calculated for a range of different values of the primary particle diameter $D_1, \ldots , D_n$, the result may be represented in a Duane plot by plotting the LII signals normalized to the signal at a specific diameter.

The drawback of the Duane plot representation is that it becomes hard to compare different cases, especially when the assumption of a power-law dependence is invalid and exponents x can not be derived. A more hands-on representation has been outlined by Mewes and Seitzman [10,11], who discussed the nonlinear dependence of LII signal on soot volume fraction as part of an investigation of systematic errors introduced when calibrating LII. They expressed the deviations from a linear relationship by calculating the relative error with regards to a reference diameter,

corresponding to the conditions in a calibration point in a flame. Following Mewes and Seitzman [11] a proportionality constant can be defined according to

$$C = \frac{\int_{t_1}^{t_2} S_{\text{LII}} dt}{\frac{\pi}{6} N_p D_0^3}, \tag{5}$$

where t_1 and t_2 denotes the detection gate interval and the initial particle diameter, D_0, is used in the soot volume fraction expression to avoid confusions regarding the time-dependence of the particle diameter during the process. The relative error, ε, with regards to a reference point can be written as

$$\varepsilon = \frac{C_{\text{test}} - C_{\text{ref}}}{C_{\text{ref}}}, \tag{6}$$

where C_{test} is the calibration constant for the test case and C_{ref} is the calibration constant for the reference case. Experimentally, this relative error will be introduced solely due to a size difference when evaluating soot volume fractions in a test region (with particle size D_{test}) by linear extrapolation to the signal obtained in a reference region with known soot volume fraction (particle size D_{ref}). The relative error defined in Eq. 6 is defined for time-integrated (gated) detection. The proportionality constant and relative error may also be calculated time-resolved and in this case the integral is removed in (5) to form

$$C'(t) = \frac{S_{\text{LII}}(t)}{\frac{\pi}{6} N_p D_0^3}, \quad \varepsilon'(t) = \frac{C'_{\text{test}}(t) - C'_{\text{ref}}(t)}{C'_{\text{ref}}(t)}. \tag{7}$$

Instead of comparing the total time-integrated LII signal the signal is compared as function of time. Studying the time-resolved relative error enables determination of the influence of the gate time and delay on the relative error and is hence primarily intended as a tool for wisely choosing these parameters.

3   Results and discussion

A number of parameters describing physical conditions and properties of the experimental setup will be varied in the model for LII in order to investigate its influence on the size dependence. These variations will be made in comparison with one base case described in Table 1. The fundamental Nd:YAG laser wavelength at 1064 nm was used. This wavelength is recommended in order to avoid laser-induced interferences from molecular species [5,18]. The temporal profile is modelled as Gaussian with the full width at half maximum (FWHM) at 8 ns and the spatial profile is top-hat. Two laser fluence values are used: One low-fluence value at 0.1 J/cm^2 predicting typical maximum particle temperatures of ~3100 K, and one high-fluence value at 0.4 J/cm^2 with a predicted reduction of the particle diameter to ~85% of its initial value. Detection is at 500 nm using a 20 ns gate centred on the laser pulse, and the gas temperature and pressure is 1800 K and 0.1 MPa respectively. The primary particle size distribution is monodisperse and the particles are assumed not to be aggregated.

3.1   The validity of the Melton expression

When Melton [3] derived the well-known expression given here as Eq. 2, he assumed that the absorption and sublimation rates were the dominating mechanisms, an assumption that may be valid at high laser power. He arrived at a power-law dependence between the signal and the particle size due to the fact that exponential functions occurred in both the Clapeyron equation for the vapour pressure he used within the sublimation term, and in the Planck radiation law as part of the signal expression. As will be shown later, other dependencies are readily found for conditions where Melton's assumptions do not apply. However, in this section the power-law dependence is assumed, and the aim is to establish if the Melton expression can be used to describe the data obtained from the present model using the complete set of functions and parameters without any simplifications.

In Fig. 3a the time-integrated LII signal is shown as function of the primary particle diameter for the base case with varying detection wavelengths in a log-log representation. The laser fluence is kept relatively high at 0.4 J/cm^2 to ensure high sublimation, and the spatial profile of the laser is top-hat. The experimental conditions are here close to those used by Melton, and the straight lines do suggest a power-law dependence. The exponents x for the different detection wavelengths are also shown. The exponent has been derived both by fitting the model results to a power law using a fitting scheme based on the Trust-Region Reflective Newton method, and by directly applying the Melton expression (Eq. 2). As can be seen, the values are in good agreement, which from a model perspective may result from the close relationship between our current model and the original Melton model with respect to the sublimation mechanism.

The exponent x increases for shorter detection wavelengths, as shown in Fig. 3. Since this wavelength only occurs in the signal expression (See Eq. 3), the deviations have its origin in this term. However, as mentioned in the last section, it is important to note that the detection wavelength only scales the influence of the temperature T originating from the heat and mass balance equations. Any deviation from linearity between LII signal and f_v requires some of the terms in the energy balance to have other than volume dependence. A simple test disabling the heat conduction term, and using low fluence to avoid sublimation (this would be the ideal representation of LII experiments in ultra-high vacuum as recently investigated by Beyer and Greenhalgh [19]) results in linearity between LII signal and f_v for all investigated detection wavelengths as a result from the temperature being derived using an energy balance only containing volume-dependent terms.

Figure 3b shows the results obtained when delaying the detector gate 100 ns. Clearly this represents a situation for which the Melton expression does not apply, and the curved lines show that the power-law assumption no longer holds. Moreover, the non-linear relationship is increased as compared to Fig. 3a. The dependencies shown in
Fig. 3a-b do differ, but it is interesting to note that for increasing primary particle diameters, the curves seem to converge to power-law dependence also for Fig. 3b.

3.2   A parameter study

As discussed in the previous section, the results in Fig. 3 indicate that the power-law assumption of Melton with the exponent x often discussed in the literature can not be used to describe the general case. Instead the relative error will be used to represent the relationship between LII signal and particle size. As discussed earlier, this error is defined with respect to a reference point, in this case corresponding to a certain

primary particle size. In the results presented in this section the reference point will be constantly defined to a primary particle size of 20 nm.

Figure 4a shows the relative error defined in Eq. 6 calculated for the base case previously shown in normalised log-log representation in Fig. 3a. Even for these experimental conditions generally considered well suited for soot volume fraction measurements, the systematic errors in soot volume fraction may be quite large. The influence of these errors will be larger for systems in which a large range of particle sizes occur, like for instance for soot volume fraction imaging of practical flames in which nucleation regions with particle sizes of a few nanometres are present as well as regions with aggregated particles with primary particle sizes of around 50 nanometres. For delayed detection (Fig. 4b) the relative errors are approximately a factor of 2 larger for the chosen detection delay of 100 ns, the same case previously shown in Fig. 3b. As previously mentioned, the detection wavelength acts as a scaling factor that influences the non-linearity of the signal, making the merits of using longer detection wavelengths clear.

The original Melton expression was derived for high-fluence conditions. Since LII measurements of soot volume fraction sometimes also are performed in the low-fluence regime, it becomes of interest to determine how the laser fluence affects the size effect on the relation between LII signal and soot volume fraction. In Fig. 5a the relative error is shown as function of primary particle diameter for the base case with varying laser fluence. It is obvious that the laser fluence has substantial impact on the relative error and that the moderate- to high-fluence regime where soot volume fraction measurements usually are carried out seems less good from this aspect. Noticeable is also the strong increase of the error for small particle sizes. In Fig. 5b the time-resolved error for the same case is shown. What seems to distinguish the low- from the high-fluence case is the initial increase of the error during the laser pulse. This behaviour for high fluence was previously predicted by Mewes et al. [11] and mainly results from the influence of the sublimation term during the laser pulse essentially creating a size dependence of the maximum particle temperature. Going back once more to Fig. 2, this can be clearly seen in the modelled temperatures for the high-fluence case (Fig. 2a) while the maximum temperatures for the low-fluence case (Fig. 2b) show much smaller size dependence. For all fluences, the error increases with time, a result from the dominating process in this regime, the heat conduction. These results suggest that low-fluence LII detected using a short prompt gate only introduces small deviations from linearity between LII signal and soot volume fraction.

Some experimental work may support these findings. Vander Wal and Jensen [20] performed LII measurements over a large range of fluences in a laminar ethylene jet flame comparing their results with extinction measurements in the same flame. They found best agreement at the lowest fluence 0.18 J/cm^2, which, predicted by our own model, yields negligible mass loss when excited using 1064 nm. There are, however, uncertainties in the results by Vander Wal and Jensen, since some may have been introduced due to the deconvolution of the extinction data, and their results may not indisputably be attributed to improved linearity at lower fluences. Additionally, LII model predictions in the high-fluence regime are still uncertain due to the partly unknown physical processes, and though the results in Fig. 5 are likely to be indicative of the real case, the results at higher fluence may in reality be different due to the influence of other loss mechanisms, such as photodesorption or oxidation [16]. Also, it must be noted that the nearly linear relationship between the LII signal and f_v at low fluences is predicted when using a model for the particle emissivity within the

Rayleigh limit where the emissivity has a linear dependence on the primary particle size essentially giving them the same maximum temperature. For large particle sizes, especially when using 532 nm excitation, the emissivity deviates from the Rayleigh expression and must be treated using the full Mie theory as recently highlighted by Liu et al. [21]. This is however not included in the present work.

The results in Fig. 5 were derived using the assumption of a uniform spatial profile of the laser beam, whereas LII experiments in practical devices often are carried out using a non-homogeneous profile. The fluence-dependence effect (discussed in relation to Fig. 5) will thus be averaged depending on the shape of the distribution function for the laser profile. Figure 6 shows the diameter dependence of the LII signal for three different spatial beam profiles: The top-hat, the Gaussian sheet (uniform distribution as function of height and Gaussian as function of width) and the Gaussian beam (See Fig. A2). The curves have been calculated for the same value of the mean laser fluence, i.e. the laser pulse energy divided by the cross section area defined using the $1/e^2$ diameter for the Gaussian function.

A comparison of Fig. 6a and b shows that the influence of the beam profile is small compared to the influence of the mean laser fluence. A somewhat larger difference between the curves can be seen in the low-fluence results in Fig. 6a. While the top-hat profile only contains one specific laser fluence, the non-uniform profiles will cover fluences ranging from zero at the boundaries of the Gaussian function up to a peak laser fluence at the centre of the beam. Moreover, in the present comparison, the mean fluence, F_{mean}, is kept constant for the three spatial profiles, meaning that the individual values of the peak fluence, F_{peak}, of the compared profiles will be different, ranging from equal to the mean fluence for the top-hat profile, $(8/\pi)^{1/2} \approx 1.59$ times the mean fluence for the Gaussian sheet and 2 times the mean fluence for the Gaussian beam. In view of the results shown in Fig. 5a it might not be too surprising that the Gaussian beam, with fluence values a factor of 2 stronger than the ones for the top-hat profile it is being compared to, will give rise to larger relative errors. However, things are complicated by the fact that a trade-off effect will be introduced due to the relative weights of the fluence regimes in the respective profile. The strong peak fluences of the Gaussian beam will only occur in a limited region at the centre of the beam whereas the peak fluence in the top-hat profile will be the same for the whole cross-section area. This effectively reduces the increase of the error expected when only taking into account the difference in peak fluence. The ideal case without a trade-off effect can actually be seen in Fig. 5a for the top-hat profile and the corresponding increase of a factor of 2 (going from 0.1 to 0.2 J/cm^2) shows a much larger increase of the relative error.

Figure 6b shows the comparison for a higher mean fluence, 0.4 J/cm^2. For this laser fluence the trend is opposite to the one seen in the low-fluence case of Fig. 6a, and the smallest relative errors now occur for the Gaussian beam. This can be explained by the fact that the increase in relative error as function of fluence is very limited in the high-fluence regime as can be seen in Fig. 5a, where an increase from 0.2 to 0.5 J/cm^2 only shows a moderate increase of the error. The small increase of the relative error predicted from the spatially limited high-fluence regions of the non-uniform profiles can not counteract the strong decrease of the error at lower fluences in the wings of the profile, and the trade-off effect in this case works in the opposite direction as compared to the low-fluence case of Fig. 6a.

The influence of the spatial profile on LII signals in general is discussed by Schulz et al. [2]. For time-resolved laser-induced incandescence, where the LII signal decay is used to infer particle size information, a top-hat profile is recommended since it will

enable heating of the particles to essentially the same maximum temperature. However, for soot volume fraction measurements, the high-fluence domain has been extensively used in the past due to the possibilities of reaching a nearly fluence-independent signal. This feature, which has its origin in a trade-off between the signal contributions from soot in the wings of the spatial laser energy profile (moderate fluence levels and no soot sublimation) and the signal contributions from the soot in the centre of the beam (high fluence levels with soot sublimation causing mass loss) [22], enables measurements nearly unaffected by attenuation of the laser beam through the measurement region. As previously mentioned, the results shown in Fig. 5 suggest that the high-fluence regime would introduce larger uncertainties when assuming linearity between LII signal and volume fraction and that low-fluence LII measurements therefore are encouraged. On the other hand, such measurements will be highly dependent on the local laser fluence introducing large uncertainties if not properly compensated for. The results in Fig. 6 suggest that the LII signal to soot volume fraction relationship will be marginally affected by the choice of spatial profile of the laser beam in the high-fluence regime, enabling straight-forward compensation on the measurement data if size information can be estimated.

All results shown so far have been derived for atmospheric flame conditions. As the LII technique is readily applied in high-pressure conditions such as internal combustion engines, the pressure influence becomes important. The most prominent difference between high-pressure applications and those at atmospheric pressure is the much stronger heat conduction [23], which is expected to increase the relative errors when assuming linearity between LII signal and f_v. In Fig. 7a the relative error is shown for varying pressure for the base case at 0.4 J/cm^2. As can be seen the deviation from a linear relationship between LII signal and soot volume fraction is increasing with pressure. The time-resolved errors are shown in Fig. 7b for a particle size at 30 nm with respect to a reference at a size of 20 nm. The relative error initially shows a plateau behaviour and during the first 10-15 ns of the LII signal duration, the relative error never exceeds 20%. The time-resolved relative errors for the low-fluence case at 0.1 J/cm^2 is shown in Fig. 7c. A comparison with the high-fluence case in Fig. 7b reveals that the relative error for the low-fluence case during the time when the LII signal is strong is substantially higher than at the high fluence. Additionally, the near-plateau behaviour seen for the high-fluence case can not be seen for the low-fluence case, where the relative error increases constantly with time. The reason for this behaviour is the two competing loss mechanisms heat conduction and sublimation, which have quite different pressure dependence. While the heat conduction term scales approximately linear to pressure, the sublimation term is slightly decreasing with pressure due to the predicted reduction of carbon flux from the surface of the particles in the continuum regime (See Eq. A.16). For the high-fluence case, sublimation will have a substantial impact on the signal and hence the nonlinearity during and somewhat after the laser pulse effectively reducing the influence of the heat conduction process. At low fluence, sublimation is not contributing to the energy loss rates, which means that essentially the whole energy loss occurs via the heat conduction process, heavily increasing the relative error as function of pressure. At times after the end of the laser pulse, the non-linearity increases heavily for all fluences.

One interesting feature in Fig. 7b is that the relative error shows pressure dependence also during the laser pulse. This would mean that attempts to calibrate for instance in-cylinder LII data recorded using a short prompt gate by using an atmospheric flame burner would introduce errors in the measurements even in the

case of equal particle sizes in the two systems. We have in a previous study derived this error as function of gate width and, provided that a short prompt gate is used, the relative error was found to be less than 30% for the investigated experimental conditions [24], and proposed compensating these errors by taking the effect into account during soot volume fraction quantification. By knowing the complete behaviour of the relative error as function of both pressure and diameter makes it possible to compensate the data for both the particle-size effect and the pressure effect simultaneous provided that size-distribution data is available.

There is currently a lack of experimental results with which to compare these predictions. Hofmann et al. [23] presented combined LII and extinction measurements in a high-pressure burner between 1 and 15 bar. Although the authors attained reasonable proportionality between soot volume fractions derived from LII and extinction for all investigated pressures, strong deviations occurred at fixed pressure when changing height above burner, equivalence ratio or gas velocity. The authors address this issue and discuss a number of factors that may explain these deviations, among them the particle size influence on the LII to f_v relationship. Unfortunately it could not be established whether the deviations had its origin in the LII or the extinction data, effectively reducing the possibilities of estimating the particle size effect. Comparative measurements in high-pressure burners using LII and extinction techniques are also easily influenced by the change of soot morphology with pressure, which has been discussed recently by Thomson et al. [25]. As soot particles grow larger the assumption of negligible scattering may be violated, and the results may overpredict the soot volume fraction measured by extinction. Though these and other experimental uncertainties make careful investigations of particle-size effects in high-pressure conditions challenging, such work is greatly encouraged considering the growing number of publications where LII has been applied in high-pressure conditions.

All data shown so far has been derived for single soot particles without contact with other particles. In real systems the soot particles tend to form aggregated structures thus effectively reducing the heat conduction process due to the shielding effect [26,27]. Figure 8a shows the dependence between the LII signal and the particle size for the base case at low fluence (0.1 J/cm^2) assuming different degrees of aggregation, where N_p is the number of particles per aggregate. Apparently the influence of aggregation is minor. Calculations for higher fluences, not shown here, indicate that aggregation only has marginal influence on the results. Aggregation thus seems to have a weak influence on the size dependence for atmospheric flame conditions. The small decrease in the predicted error shown in Fig. 8a for increased level of aggregation has its origin in the heat conduction term being weakened due to the shielding effect. For elevated pressure, where the heat conduction is stronger, the effect of aggregation will become more important. This is shown in Fig. 8b and c where the error due to nonlinearity at a position where the particle sizes are 30 nm is shown for a low (0.1 J/cm^2) and high fluence (0.4 J/cm^2) case, respectively. Since aggregation decreases the relative importance of heat conduction on the signal, it has a positive effect on the linearity between LII signal and soot volume fraction, most noticeable for high pressures and low laser fluences.

LII measurements are sometimes carried out at lower gas temperatures than those usually found in flames. As heat conduction is highly dependent on the temperature of the surrounding gas, influence on the size dependence in the LII to f_v relationship is expected. The flame temperature will not only affect the heat conduction, but also the amount of laser energy that is needed to reach a certain maximum particle temperature

11

during the heat-up process. For studies of the effect of varying flame temperature, one of two approaches may therefore be followed. The fluence may be kept constant corresponding to a comparison of soot volume fraction data obtained using the same experimental setup but in different local gas temperatures, occurring for instance when conducting imaging measurements at different crank angle degrees inside the combustion chamber of a Diesel engine. The other approach is to adjust the laser fluence according to the gas temperature in order to reach the same maximum particle temperature. This would correspond to an experimentalist choosing the appropriate laser fluence in the measurement region of choice. The comparison of the base case using different flame temperatures shown in Fig. 9 has been derived following the second approach, and the laser fluence has been increased for the lower gas temperatures in order to reach the same maximum temperature of the particles for all compared temperatures. Given that the size effect (of the LII signal on soot volume fraction) will be dependent on the maximum particle temperature, the adjustment of laser fluence has only been undertaken for the reference particle size of 20 nm, and the fluence value used for different particle sizes for a specific gas temperature is kept constant, enabling different particle sizes reaching somewhat different maximum temperatures for that specific gas temperature. The location of the maximum temperature inevitably shifts to later times for lower gas temperatures, due to the increased duration of the heat-up process, but the difference is only ~1.2 ns between the 300 K and 1800 K case. Figure 9a shows the influence of gas temperature on the error at a low fluence of 0.1 J/cm^2 at 1800 K. As can be seen, the lower gas temperature has a negative impact on the linearity between LII signal and soot volume fraction. At these low fluences sublimation has no impact on the result and increased importance of the heat conduction term will solely be responsible for the introduced errors.

An increase of the laser fluence to 0.4 J/cm^2 at 1800 K and the prompt 20 ns gate results in practically no difference as function of temperature (not shown in figure). The time-resolved error for this high-fluence case is shown in Fig. 9b. Obviously the region centred on 20 ns is quite unaffected by changes in temperature whereas the early region and the region after the pulse show increased errors similar to what was found for the pressure influence shown in Fig. 7. This is again encouraging for soot volume fraction measurements in the plateau regime, especially in systems with strong deviations of local gas temperatures like for instance crank-angle resolved measurements in Diesel engines [28].

3.3 Investigations for real experimental conditions

The parameter study presented in the last section clearly shows the influence of the different terms with respect to the size dependence of the LII signal to f_v relationship. It would, however, be useful to see estimations of the influence for realistic measurement situations where the conditions are much more complex than in the parameter study. Previous studies from literature will form a basis for this investigation. Soot volume fraction imaging using LII was carried out in internal combustion engines already during the early 90's and on the whole, the praxis does not seem to have changed that much during the years to come for similar applications in harsh environments. Typically high laser fluences and non-uniform spatial profiles of the laser beams were used creating a plateau regime in the power dependence of the LII signal decreasing the uncertainties introduced by high laser attenuation and shot-to-shot fluctuations. A prompt gate was used together with broadband detection. The

experimental characteristics of the work by Dec [29] serves as foundation for a realistic base case in the following study. The data is presented in Table 2 and the corresponding relative error is shown in Fig. 10a for 0.1 and 4.0 MPa, respectively, and the corresponding LII signals for a particle size of 30 nm is shown in Fig. 10b together with the laser pulse and the 70 ns gate. The relative error has been derived for two different gas temperatures (1200 K and 2200 K). No adjustments were made for the laser pulse energy when making this comparison, since it, contrary to the case presented in Fig. 9, represents different temperatures occurring for the same experimental setup. The trends previously visualised in Figs 7 and 9 are clearly seen also for this real case. The relative errors increase with increasing pressure and approach a factor of 2 for the investigated range of diameters and a reference particle size of 20 nm. The influence of gas temperature is lower but cool regions are predicted to give somewhat larger errors than hot. Considering the large uncertainties involved in measurements in internal combustion engines with respect to laser attenuation and signal trapping [24,30] this error may not be the most important. The fact that larger particles contribute to the LII signal much more than smaller ones also means that relatively large errors for small particles will be less important in areas with large distributions of both small and large particle sizes. If, however, measurement data is compared to that obtained in a calibration source in which substantially smaller particles are present, quantitative data may suffer from large uncertainties.

One interesting question arises with regards to the previous investigation, and that concerns the detection gate. It is not uncommon to have interferences during and somewhat after the laser pulse due to fluorescence or scattering and this may give rise to large uncertainties in the results [2]. The long decay time of the LII signal at atmospheric pressure makes it possible to achieve reasonable signal-to-noise ratio also with delayed gating and this scheme has been used both in flames [31] and in different combustion devices [32,33]. However, at elevated pressures the decay time is drastically shortened due to the increased particle energy loss due to heat conduction, as can be seen in the theoretically calculated signals shown in Fig. 10b. To estimate how typical delay times affect the LII signal, the delay of the 70 ns gate in the realistic case based on prompt detection (See Table 2) was varied in order to estimate the influence on the relative error. The error at a particle size of 30 nm with respect to the reference size of 20 nm is shown in Fig. 11a for the two different choices of ambient gas pressure and temperature. As the LII signal strength decreases after the laser pulse, LII measurements using delayed detection will be limited to delay times short enough for attaining a sufficient signal-to-noise ratio. A discussion regarding the LII signal to soot volume fraction relationship for delayed detection will thus not be complete without knowledge on the collected absolute signal. Therefore the fraction of the signal intensity compared to the total signal collected from 0 to 300 ns is shown together with the laser pulse in Fig. 11b. Due to the relatively long gate (70 ns) strong deviations do not occur until a delay of 30 ns where the gate opens at the start of the laser pulse. For shorter delays the complete prompt signal is collected and the small evolutions with delay timing are attributable to the increased portion of delayed signal detected. This is especially evident in Fig. 11b for 0.1 MPa where the signal fraction increases as function of delay time up to about 30 ns. For delays between 30 and 40 ns the relative error increases and the detected signal fraction decreases. This is the intermediate region where the gate only captures parts of the prompt signal. At a delay time of 45 ns the laser pulse has ended and complete delayed detection is used. For the atmospheric case (0.1 MPa) the relative error increases from ~15% to ~25% for

the 1200 K case and even less for the 2200 K case. A further increase in delay time not shown here does not strongly increase the error and at a delay of 100 ns (corresponding to 65 ns after the end of the laser pulse) the error is still below 50% for the 1200 K case. For the high-pressure case (4 MPa) the error increases heavily with increasing delay time and is predicted to be approaching 200% for the 1200 K case already at the end of the laser pulse at ~45 ns. At this position only about 5% of the total LII signal is detected as can be seen in Fig. 11b. For delay times tens of nanoseconds after the laser pulse the present investigation indicate an extremely low detected fraction of the total signal and a heavily nonlinear relationship between the LII signal and soot volume fraction. These results, though maybe not too surprising considering the fact that the late parts of the signal decay is highly dependent on the particle size, do put some questions as to the quality of soot volume fraction measurements in high pressure environment using delayed gates, like for instance reported in [32]. However, it must be remembered that for some experimental conditions the problem with interfering light from scattering and fluorescence can be so problematic that a delayed gate has to be chosen although the quantitative information becomes worse. The same consideration can be mentioned regarding the choice of a short detection wavelength for the LII signal. Sometimes a detection wavelength of 400-450 nm must be chosen to effectively suppress the background flame luminosity despite the fact that it leads to increased non-linearity between the LII signal and soot volume fraction.

We end this section by noting that at conditions in practical devices, especially in highly fluctuating systems like in Diesel engines, some parameters like for instance the detection wavelength and gate and the laser fluence may be controlled, while others, like the gas temperature and pressure, may not. In view of the results presented in the last section and indeed also Fig. 10, it may be concluded that variations in the uncontrolled parameters will not affect the relative error to a great extent provided that the controlled parameters are chosen wisely, especially the choice of detection gate timing. Provided that a short prompt gate is used the relative error is only moderately dependent on the ambient gas temperature and pressure. Though the uncertainty is likely to increase somewhat in evaluated relative errors, and hence also in evaluated soot volume fraction after compensating for the particle size effect, this increase may be considered acceptable.

4   Conclusions

An extensive theoretical investigation of the relationship between the LII signal and the soot volume fraction has been carried out, where the influence of variations in particle size has been investigated. A heat and mass transfer model for laser-heated soot particles was applied in order to predict the LII signal dependence on a large number of physical and experimental parameters, and these results were used to predict the errors introduced during measurements at different conditions when assuming perfect linearity between the LII signal and the soot volume fraction. The results are the following:

1.   The expression derived by Melton stating that the signal is proportional to the particle diameter raised to the power of $3+0.154/\lambda_{det}$ (λ_{det} in microns) was verified for a prompt gate with duration of 20 ns and a laser fluence of 0.4 J/cm^2 at 1800 K and 0.1 MPa.

2. For LII applications, it is desired that there is a linearity between LII signal and soot volume fraction, f_v, without any particle size influence on this relationship. To minimize such an effect, it is beneficial to use short prompt gates, and longer detection wavelengths.

3. For atmospheric flame conditions, the particle size influences the relationship between prompt LII signal and f_v to a low degree in the low-fluence regime, but has a clear influence in the high-fluence regime.

4. The spatial beam profile (Top-hat, Gaussian sheet or Gaussian beam) has little effect on the relationship between LII signal and f_v for variations in particle size in the high-fluence regime. From a size-dependence point of view of linearity between LII signal and f_v, there is no reason of using a top-hat profile when measuring soot volume fraction at high fluence. At lower fluences the spatial profile shows a somewhat higher impact.

5. Increased pressure increases the non-linearity between LII signal and f_v for variations in particle size, also when using prompt detection. From this point of view, the high-fluence regime is recommended for high pressure measurements as the sublimation process competes with the heat conduction effectively reducing the pressure influence on the non-linearity during the first 10-15 ns of the LII signal.

6. Aggregation of particles has little impact on the relationship between LII signal and f_v for variations in particle size at atmospheric pressure, and also at increasing pressures in the high-fluence region, whereas the impact is higher in the low-fluence region. A high degree of aggregation is predicted to decrease the uncertainties introduced due to the size dependence as it decreases the heat conduction rate.

7. The particle size influences the non-linearity between LII signal and f_v more for decreasing ambient temperature.

8. By studying the time-resolved LII signals for different particle sizes, a detailed understanding of the particle size effect on the LII signal dependence on f_v could be obtained. The main reason for this influence is that the heat conduction is area dependent rather than volume dependent.

9. A realistic case based on the experimental setup and conditions presented by Dec [29] was investigated and it was found that the 70 ns gate centred on the laser pulse and at a pressure of 4 MPa resulted in an overprediction of soot volume fraction a factor of ~2 when comparing particle diameters of 60 nm in comparison with 20 nm.

10. Low-fluence LII conducted in atmospheric flame conditions has in this study shown a more close-to-linear relationship between LII signal and f_v for variations in particle size. However, the sensitivity of the signal to pulse-to-pulse fluctuations of the laser energy and beam attenuation makes low-fluence LII less useful for visualisation of soot in practical devices. Additionally, comparing the pressure dependence of the relative error derived for the low-fluence and high-fluence case indicates that low-fluence LII introduced larger errors at elevated pressures.

11. High-fluence LII shows a relatively high influence of particle size on the relationship between LII signal and f_v, where volumes with big particles lead to

overestimations of soot volume fractions. Using prompt detection with a short gate, this relationship is relatively unaffected by variations in spatial beam profile, aggregation, and background temperature and pressure. This means that if local particle sizes can be extracted simultaneously with local soot volume fractions in a visualisation experiment, this information could be used to compensate the local soot volume fractions and thereby improve the accuracy in the quantitative soot volume fraction measurements.

The focus of this investigation has been to explore the relationship between the LII signal and the soot volume fraction when considering different particle sizes. In a real experimental situation this is one factor to consider when choosing experimental parameters. Others are, for instance, beam and signal attenuation, avoidance of fluorescence effects, and suppression of background luminosity.

Appendix A: The model for laser-induced incandescence

In this Appendix the theoretical model used for predicting the LII signal response for a particular measurement volume and experimental setup will be presented. The nomenclature defining the functions and parameters as well as the values used in this study is given in Appendix B.

The model for LII is based on the one proposed by Melton [3], Hofeldt [34] and Snelling et al. [15] and is an updated version of the model presented in [35] and [22]. The core of the model is two differential equations, where the first contains the energy balance and the second the mass balance. The energy balance equation can be written according to

$$\dot{Q}_{abs} - \dot{Q}_{cond} - \dot{Q}_{sub} - \dot{Q}_{rad} - \dot{Q}_{int} = 0 \,. \tag{A.1}$$

The rate of absorbed energy is modelled using the Rayleigh-Debye-Gans theory for poly-fractal aggregates (RDG-PFA), which states that the absorption and radiation properties of aggregates can be expressed as the sum of the same processes for individual primary particles [2]. This assumption is believed to be true for fractal aggregates [36] used in the investigations presented in this paper. The absorption rate will thus resemble the Rayleigh limit expression and may be written as [16,37]

$$\dot{Q}_{abs} = \frac{\pi^2 D^3 E(m) N_p F}{\lambda} g(t) \,, \tag{A.2}$$

where $g(t)$ is the normalized temporal distribution of laser energy of the incoming laser pulse.

Since the heat conduction is a crucial loss mechanism with regards to the size dependence of the LII signal, it is of utmost importance to treat this process accurately. In this work we have used the Fuchs heat conduction model [38-40], recently suggested to be the most accurate formulation for spherical nano-particles especially for high pressures and low gas temperatures [40]. Heat conduction is

dependent on the effective area available for heat transfer, which will be dependent on the level of aggregation among the soot particles. One way of accounting for this can be done by introducing an equivalent heat conduction diameter, D_{HC}, which is defined as the diameter of an equivalent single solid sphere that has the same energy transfer surface area as the aggregate [26]. In this work we follow the approach outlined by Liu et al. [27] where the relation between this diameter and the primary particle diameter is given by

$$\begin{cases} D_{HC} = D, & N_p = 1 \\ D_{HC} = \left(\dfrac{N_p}{k_h} \right)^{1/D_h} D, & N_p > 1 \end{cases} \tag{A.3}$$

where the scaling constants k_h and D_h were determined as functions of the thermal accommodation coefficient α using direct simulation Monte Carlo (DSMC). The simulations were carried out by Liu et al. [27] for free molecular regime conditions and aggregate sizes with N_p spanning the interval 1-199, using the description of the fractal properties of the aggregates given by Filippov et al. [41]. The DSMC results were fitted with second-order polynomials resulting in

$$\begin{cases} k_{h,FM} = 1.04476 + 0.22329\alpha + 7.14286 \times 10^{-3}\alpha^2 \\ D_{h,FM} = 1.99345 + 0.30224\alpha - 0.11276\alpha^2 \end{cases}. \tag{A.4}$$

For a thermal accommodation coefficient of 0.3 used in this work, the scaling constants will be $k_{h,FM} = 1.112$ and $D_{h,FM} = 2.074$.

The Fuchs heat conduction model is a two-layer model where the space surrounding the soot particle is divided into an inner and an outer region separated by a limiting sphere. Inside this sphere, heat conduction is treated according to free molecular regime theory, and outside according to continuum regime theory. This is depicted in Fig. A1. Please note that the equivalent heat conduction size is defined using the radius $a_{HC} = D_{HC}/2$. Two extra variables are defined for this geometry, one representing the distance between the soot particle and the limiting sphere, δ, and one representing the temperature inside the sphere, T_δ. The heat conduction within the sphere is modelled according to

$$\dot{Q}_{FM} = \frac{1}{2}\alpha\pi a_{HC}^2 p \sqrt{\frac{8k_B T_\delta}{\pi m_g}} \frac{\gamma^* + 1}{\gamma^* - 1}\left(\frac{T}{T_\delta} - 1\right), \tag{A.5}$$

where the mean heat capacity ratio γ^* is defined given as

$$\frac{1}{\gamma^* - 1} = \frac{1}{T - T_\delta}\int_{T_\delta}^{T}\frac{dT}{\gamma - 1}. \tag{A.6}$$

in which $\gamma = C_p/C_v = C_p/(C_p - R)$ is the heat capacity ratio. The heat conduction outside of the sphere is expressed as

$$\dot{Q}_C = 4\pi(a_{HC} + \delta)\int_{T_g}^{T_\delta} k_g \, dT. \tag{A.7}$$

The distance δ is given as

$$\frac{\delta + a_{HC}}{a_{HC}} = \frac{a_{HC}^2}{\lambda_\delta^2}\left(\frac{1}{5}\Lambda_1^5 - \frac{1}{3}\Lambda_2\Lambda_1^3 + \frac{2}{15}\Lambda_2^{5/2}\right),\tag{A.8}$$

where the mean free path inside the limiting sphere, λ_δ, is related to the mean free path of the gas according to

$$\lambda_\delta = \frac{k_g(T_\delta)}{k_g(T_g)}\sqrt{\frac{T_\delta}{T_g}}\left(\frac{\gamma(T_\delta)-1}{\gamma(T_g)-1}\right)\frac{f(T_g)}{f(T_\delta)}\lambda_g,\tag{A.9}$$

assuming that the pressure is the same within and outside of the sphere. The functions within brackets in (A.8) are defined in the expressions

$$\begin{cases}\Lambda_1 = 1 + \lambda_\delta/a_{HC}\\[2mm]\Lambda_2 = 1 + (\lambda_\delta/a_{HC})^2\end{cases}.\tag{A.10}$$

The mean free path of the gas is given by [40,42]

$$\lambda_g = \frac{k_g(T_g)}{f(T_g)p}\left(\gamma(T_g)-1\right)\sqrt{\frac{\pi n_g T_g}{2k_B}},\tag{A.11}$$

where $f = (9\gamma - 5)/4$ is the Eucken correction for the thermal conductivity of polyatomic gases [16]. By utilizing the fact that no other heat source exist than the particle itself, continuity states that the expressions in Eqs. A.5 and A.7 should give equal values at the limiting sphere boundary. The balance equation created by this boundary condition together with Eq. A.8 makes it possible to numerically solve the problem for a predefined equivalent heat conduction radius a_{HC} and particle temperature T at the conditions defined by the ambient gas temperature T_g and pressure p. This operation is carried out prior to solving the heat and mass balance equations of the LII process, and must therefore be made for an appropriate range of values for the particle size and temperature, since these are variables in the model for LII.

The sublimation term is derived for an average ensemble of sublimed carbon species ($C_1, \ldots, C_7$) and is based on the treatment presented by Hofeldt [34], Snelling et al. [15] and Smallwood et al. [43]. Like the heat conduction term, the sublimation term is essentially area-dependent, and it is therefore reasonable to assume that aggregation will affect the influence of the process. However, to the authors' knowledge no thorough investigation has been presented which suggests that the scaling law previously described for the heat conduction can be used also for sublimation, and even if it can, the scaling constants must be determined for the sublimation process. The choice has therefore been made to use the total area of the primary particles in this work, something that may overpredict the influence of sublimation for aggregated particles. From this follows that the rate of energy loss from an aggregate can be written according to

$$\dot{Q}_{sub} = -N_p\frac{\Delta H_v}{M_v}\frac{dM}{dt},\tag{A.12}$$

and the mass rate from one primary particle of mass M can be written as

$$\frac{dM}{dt} = -\pi D^2 N_v\frac{M_v}{N_A}.\tag{A.13}$$

The molecular flux of sublimated carbon, N_v, can be expressed for the transition regime by using a simple harmonic mean expressed as

$$N_v = \left(\frac{1}{N_C} + \frac{1}{N_{FM}} \right)^{-1} , \tag{A.14}$$

where the expression for the free molecular regime is given as

$$N_{FM} = \beta n_v \sqrt{\frac{RT}{2\pi M_v}} , \tag{A.15}$$

and the continuum regime expression as

$$N_C = 2 n_v \frac{\Gamma_{diff}}{D} . \tag{A.16}$$

Here β is the mass accommodation coefficient in this work assumed to be 0.8 [15] and Γ_{diff} the diffusion coefficient, for which the expression given by Michelsen [16],

$$\Gamma_{diff} = \frac{f k_B T}{4 \sigma p} \sqrt{\frac{RT}{\pi M_v}} , \tag{A.17}$$

is used. Using the ideal gas equation the molecule number density of soot vapour can be written as

$$n_v = \frac{P_v N_A}{RT} . \tag{A.18}$$

The mass rate may thus be written according to

$$\frac{dM}{dt} = -\pi D^2 P_v \sqrt{\frac{M_v}{2\pi RT}} \left[\frac{\sqrt{2} D \sigma p}{f k_B T} + \frac{1}{\beta} \right]^{-1} . \tag{A.19}$$

The vapour pressure, P_v, heat of sublimation, ΔH_v, and average molecular weight of the sublimed species, M_v, are temperature-dependent functions implemented as polynomials obtained from Smallwood et al. [43]. We also note that the sublimation process is difficult to model accurately, and that further research in this area including aggregation effects is strongly encouraged.

The radiation term expressed within the limits of RDG-PFA theory may be written as [16]

$$\dot{Q}_{rad} = 8\pi^3 D^3 hc^2 N_p E(m) \left(\frac{k_B T}{hc} \right)^5 \zeta(5)\Gamma(5) = \begin{bmatrix} \zeta(5) \approx 1.0369 \\ \Gamma(5) = 24 \end{bmatrix} \approx \frac{199\pi^3 N_p D^3 (k_B T)^5 E(m)}{h(hc)^3} . \tag{A.20}$$

where ζ and Γ are the Zeta and Gamma functions respectively [16]. The internal energy change is modelled according to [3,16,34]

$$\dot{Q}_{int} = \frac{\pi}{6} D^3 N_p \rho_s c_s \frac{dT}{dt} . \tag{A.21}$$

The mass rate of one primary particle can be written as [34]

$$\frac{dM}{dt} = \frac{\pi}{2} \rho_s D^2 \frac{dD}{dt} + \frac{\pi}{6} D^3 \frac{d\rho_s}{dT} \frac{dT}{dt} , \tag{A.22}$$

which yields an expression for the rate of diameter change according to

$$\frac{dD}{dt} = \frac{2}{\pi \rho_s D^2}\left[\frac{dM}{dt} - \frac{\pi}{6}D^3 \frac{d\rho_s}{dT}\frac{dT}{dt}\right]. \qquad (A.23)$$

The equation system built from Eqs. A.1, A.19 and A.23 is numerically solved resulting in time-dependent evolutions of the primary particle temperature $T(t)$ and size $D(t)$. These functions are then used to calculate the LII signal intensity using the expression [15,16]

$$S_{LII} \propto \pi D^2 N_p \int_0^\infty R(\lambda')\frac{4\pi DE(m)}{\lambda'}\frac{2\pi hc^2}{\lambda'^5}\left(\frac{1}{e^{hc/\lambda'k_BT}-1} - \frac{1}{e^{hc/\lambda'k_BT_g}-1}\right)d\lambda', \quad (A.24)$$

given within the limits of RDG-PFA theory and where $R(\lambda)$ is a function describing the spectral sensitivity of the detection system. When predicting signals from nonuniform spatial profiles of the laser, the total LII signal is derived from a library of LII signals calculated for a range of fluence values. The weighted signal response is given as

$$S_{LII,total} = \sum_{j=1}^n S_{LII}(P_j^F \cdot E)A_j^F. \qquad (A.25)$$

Here P^F is the distribution function of laser fluence values, in this work Gaussian functions, and A^F the corresponding relative weights for each of these fluences. The weights are determined as the ratio between the cross section areas exposed to a particular fluence level (grey areas) and the total cross section area indicated in Fig. A2. The total number of sub-signals, n, for which the heat and mass transfer equations must be solved, is determined from case to case. In this work 60 calculations were found satisfactory as little real change occurred for higher values.

Appendix B: Nomenclature

a_{HC} Equivalent heat conduction radius (m), $a_{HC} = D_{HC}/2$

A^F Fraction of the total cross-sectional area of the measurement volume exposed to the specific laser fluence $P^F \times E$

c The speed of light (2.998×10^8 m/s)

c_s Specific heat of soot (J/kg K). The temperature-dependent expression for solid graphite given by Michelsen [16] is used.

C Constant of proportionality between LII signal and soot volume fraction given by Eq. 5

C' Time-resolved constant of proportionality between LII signal and soot volume fraction given by Eq. 7

C_p Heat capacity for the surrounding gas (J/mole K). The temperature-dependent expression from Michelsen [16] is used.

D Primary particle diameter (m)

D_0 The initial value of the primary particle diameter prior to heat-up (m)

D_{HC} Equivalent heat conduction diameter, i.e. diameter of a single sphere having the same heat conduction properties as that of the aggregate (m)

D_h Scaling constant for aggregate model

E Laser pulse energy (J)

$E(m)$ The absorption function, $-\text{Im}[(m^2-1)/(m^2+2)]$. Here the wavelength-dependent expression $E(m) = 0.232 + 1.2546 \times 10^5 \lambda$ from Snelling et al. [26] has been used both for the absorption (A.2) and LII signal (A.24). The radiation term (A.20) is derived assuming a wavelength-

	independent $E(m)$, and the value 0.31 was used.
f	Eucken correction for the thermal conductivity of polyatomic gases, $(9\gamma-5)/4$
f_v	Soot volume fraction given as Eq. 1
F	Laser fluence (J/m^2)
$g(t)$	Normalised temporal distribution of laser energy (s^{-1})
h	The Planck constant (6.626×10^{-34} Js)
ΔH_v	Heat of sublimation of soot implemented as a temperature-dependent expression from Smallwood et al. [43] (J/mole)
k_B	The Boltzmann constant (1.38×10^{-23} J/K)
k_g	Heat conduction coefficient of the surrounding gas (W/m K). A temperature-dependent function given by Michelsen [16] for air is used in this work, $k_g = 1.0811 \times 10^{-2} + 5.1519 \times 10^{-5}T$
k_h	Scaling constant for aggregate model
m	Refractive index of soot (not used explicitly in this study, see $E(m)$)
m_g	Average mass of gas molecules (4.78×10^{-26} kg)
M	Mass of a primary soot particle (kg)
M_v	Molecular weight of soot vapour implemented as a temperature-dependent expression from Smallwood et al. [43] (kg/mole)
n_v	Number density of soot vapour given using the ideal gas law in Eq. A.18 (m^{-3})
N	Number density of soot particles (or soot aggregates if $N_p>1$) (m^{-3})
N_A	Avogadros constant (6.022×10^{-23} mole^{-1})
N_p	Number of primary particles per aggregate
N_v	Molecular flux of sublimed carbon clusters (s^{-1}m^{-2})
N_{FM}	Free molecular regime expression for N_v given in Eq. A.15 (s^{-1}m^{-2})
N_C	Continuum regime expression for N_v given in Eq. A.16 (s^{-1}m^{-2})
p	Ambient gas pressure (Pa)
P^F	Spatial distribution function for the laser energy (m^{-2})
P_v	Vapour pressure of soot implemented as a temperature-dependent expression from Smallwood et al. [43] (Pa)
$\dot{Q}_i$	Energy rate for sub-mechanism i (J/s)
R	The molar gas constant (8.314 J/mole K)
$R(\lambda)$	Spectral characteristics of the detection system (arb. units)
S_{LII}	The LII signal (arb. units)
t	Time (s)
T	Particle temperature (K)
T_δ	The temperature inside the limiting sphere in the Fuchs heat conduction model (K)
T_g	Ambient gas temperature (K)
α	Thermal accommodation coefficient. The value 0.3 is used following Michelsen [16].
β	Mass accommodation coefficient, sometimes referred to as the evaporation coefficient. The value 0.8 is used following Snelling et al. [15]
δ	The distance between the equivalent heat conduction radius and the limiting sphere in the Fuchs heat conduction model (m)
ε	Relative error from LII measurements of soot volume fraction defined in Eq. 6
ε'	Time-resolved relative error from LII measurements of soot volume fraction defined in Eq. 7
γ	The heat capacity ratio, $C_p/(C_p-R)$
γ^*	The mean heat capacity ratio (See Eq. A.6)
Γ	The Gamma function
Γ_{diff}	Diffusion coefficient for soot vapour given in Eq. A.17 (m^2/s)
λ	Laser wavelength (m)

λ_{det} Detection wavelength in the Melton expression given in Eq. 2 (µm)

λ_g Mean free path of the ambient gas given in Eq. A.11 (m)

λ_δ Mean free path of the gas inside the limiting sphere in the Fuchs heat conduction model (m). Related to λ_g by Eq. A.9

Λ_1 Function within the Fuchs heat conduction model (See Eq. A.10)

Λ_2 Function within the Fuchs heat conduction model (See Eq. A.10)

ρ_s Density of soot (kg/m^3). The temperature-dependent expression for solid graphite given by Michelsen [16] is used, $\rho_s(T) = 2303.1 - 7.3106 \times 10^{-2} T$

σ Molecular cross section for sublimed species (m^2). The cross section for C_3 (4.5×10^{-19} m^2) given by Michelsen [16] is used.

ζ The Riemann Zeta function

References

1. R.J. Santoro, C.R. Shaddix, in *Applied Combustion Diagnostics* (Taylor and Francis, New York, 2002), p. 252
2. C. Schulz, B.F. Kock, M. Hofmann, H. Michelsen, S. Will, B. Bougie, R. Suntz, G. Smallwood, Appl. Phys. B **83**, 333 (2006)
3. L.A. Melton, Appl. Opt. **23**, 2201 (1984)
4. R.L. Vander Wal, K.J. Weiland, Appl. Phys. B **59**, 445 (1994)
5. P.-E. Bengtsson, M. Aldén, Appl. Phys. B **60**, 51 (1995)
6. B. Axelsson, R. Collin, P.-E. Bengtsson, Appl. Opt. **39**, 3683 (2000)
7. C.R. Shaddix, J.E. Harrington, K.C. Smyth, Combust. Flame **99**, 723 (1994)
8. B. Quay, T.W. Lee, T. Ni, R.J. Santoro, Combust. Flame **97**, 384 (1994)
9. T. Ni, J.A. Pinson, S. Gupta, R.J. Santoro, Appl. Opt. **34**, 7083 (1995)
10. B. Mewes, J.M. Seitzman, in *34th Aerospace Sciences Meeting*, Paper AIAA-1996-0538, Reno, NV, 15-18 January, (1996)
11. B. Mewes, J.M. Seitzman, Appl. Opt. **36**, 709 (1997)
12. R.T. Wainner, J.M. Seitzman, S.R. Martin, Aiaa J. **37**, 738 (1999)
13. D.R. Snelling, G.J. Smallwood, F. Liu, O.L. Golder, W.D. Bachalo, Appl. Opt. **44**, 6773 (2005)
14. J.E. Dec, SAE Technical Paper 970873 (1997)
15. D.R. Snelling, F. Liu, G.J. Smallwood, Ö.L. Gülder, in *Proc. 34th National Heat Transfer Conf.*, NHTC2000-12132, Pittsburg, PA, August 20-22, (2000)
16. H.A. Michelsen, J. Chem. Phys. **118**, 7012 (2003)
17. J.T. Duane, IEEE Trans. Aerospace **AS-2**, 563 (1964)
18. C.R. Shaddix, K.C. Smyth, Combust. Flame **107**, 418 (1996)
19. V. Beyer, D.A. Greenhalgh, Appl. Phys. B **83**, 455 (2006)
20. R.L. Vander Wal, K.A. Jensen, Appl. Opt. **37**, 1607 (1998)
21. F. Liu, K.J. Daun, V. Beyer, G.J. Smallwood, D.A. Greenhalgh, Appl. Phys. B **87**, 179 (2007)
22. H. Bladh, P.-E. Bengtsson, J. Delhay, Y. Bouvier, E. Therssen, P. Desgroux, Appl. Phys. B **83**, 423 (2006)
23. M. Hofmann, W.G. Bessler, C. Schulz, H. Jander, Appl. Opt. **42**, 2052 (2003)
24. H. Bladh, L. Hildingsson, V. Gross, A. Hultqvist, P.-E. Bengtsson, in *Proceedings of the 13th International Symposium on Applications of Laser Techniques to Fluid Mechanics*, Lisbon, Portugal, (2006)
25. K.A. Thomson, D.R. Snelling, G.J. Smallwood, F. Liu, Appl. Phys. B **83**, 469 (2006)
26. D.R. Snelling, F.S. Liu, G.J. Smallwood, Ö.L. Gülder, Combust. Flame **136**, 180 (2004)
27. F. Liu, M. Yang, F.A. Hill, D.R. Snelling, G.J. Smallwood, Appl. Phys. B **83**, 383 (2006)
28. J.B. Heywood, *Internal combustion engine fundamentals* (McGraw-Hill, New York, 1988)
29. J.E. Dec, SAE Technical Paper 920115 (1992)
30. K. Inagaki, S. Takasu, K. Nakakita, SAE Technical Paper 1999-01-0508 (1999)
31. F. Cignoli, S. Benecchi, G. Zizak, Appl. Opt. **33**, 5778 (1994)
32. J.A. Pinson, D.L. Mitchell, R.J. Santoro, SAE Technical Paper 932650 (1993)
33. M. Brown, T. Meyer, J. Gord, V. Belovich, W. Roquemore, in *40th Aerospace Sciences Meeting*, Paper AIAA 2002-0393, Reno NV, 14-17 January, (2002)
34. D.L. Hofeldt, SAE Technical Paper 930079 (1993)
35. H. Bladh, P.-E. Bengtsson, Appl. Phys. B **78**, 241 (2004)
36. T.L. Farias, Ü.Ö. Köylü, M.G. Carvalho, Appl. Opt. **35**, 6560 (1996)
37. C.F. Bohren, D.R. Huffman, *Absorption and scattering of light by small particles* (Wiley, New York, 1998)
38. N.A. Fuchs, P. Appl. Geophys. **56**, 185 (1963)
39. A.V. Filippov, D.E. Rosner, Int. J. Heat Mass Transf. **43**, 127 (2000)
40. F. Liu, K.J. Daun, D.R. Snelling, G.J. Smallwood, Appl. Phys. B **83**, 355 (2006)
41. A.V. Filippov, M. Zurita, D.E. Rosner, J. Colloid Interface Sci. **229**, 261 (2000)
42. B.J. McCoy, C.Y. Cha, Chem. Eng. Sci. **29**, 381 (1974)
43. G.J. Smallwood, D.R. Snelling, F. Liu, Ö.L. Gülder, J. Heat Transf. **123**, 814 (2001)

Tables and Figures

Table 1. The base case

Properties of the laser pulse	
Wavelength	1064 nm
Temporal profile	Gaussian with FWHM 8 ns
Spatial profile	Top-hat
Fluence	0.1 and 0.4 J/cm^2
Properties of the detection system	
Gate timing	20 ns centred on the laser pulse
Spectral	Single wavelength at 500 nm
Properties of the measurement volume	
Pressure	0.1 MPa
Temperature	1800 K
Aggregation	No
Primary particle size	Monodisperse distribution

Table 2. The experimental conditions of the work presented by Dec [29]

Parameter	Data given in Dec	This study
Laser wavelength	532 nm	532 nm
Temporal profile	8 ns pulse length	Gaussian profile FWHM 8ns
Spatial profile	Laser sheet (5cm × 300µm)	Gaussian sheet (5cm × 300µm ($1/e^2$))
Laser pulse energy	180 mJ/pulse	90 mJ/pulse[1]
Gate timing	70 ns centred on the pulse	70 ns centred on the pulse
Detection	Broadband detection (320 – 450 nm) using dual 450 nm short pass filters and one BG39 filter	Spectral response of detection system, $R(\lambda)$, determined from the spectral characteristics of the filters reported by Dec. Spectral sensitivity of the detector assumed wavelength-independent.
Pressure	-	0.1 and 4 MPa
Temperature	2200 K given as ref.	1200 and 2200 K
Aggregation	-	No
Primary particle size	-	The range 5 – 60 nm

[1] The mean laser fluence of a Gaussian sheet with these characteristics and the laser pulse energy reported by Dec is 1.2 J/cm^2 resulting in very high peak fluences for which the results from the current model for LII is uncertain. We have therefore chosen to use a lower pulse energy corresponding to a mean fluence of 0.6 J/cm^2
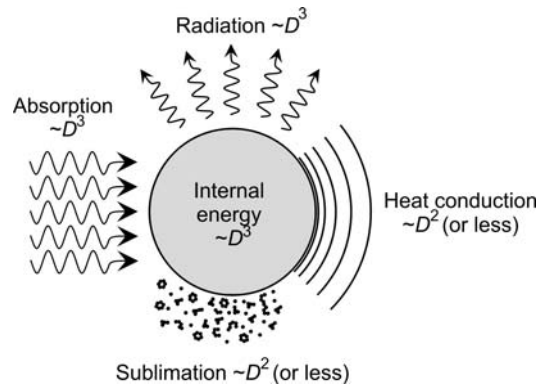
Figure 1. The physical mechanisms modelled during the LII process and their dependence on the primary particle diameter *D*.
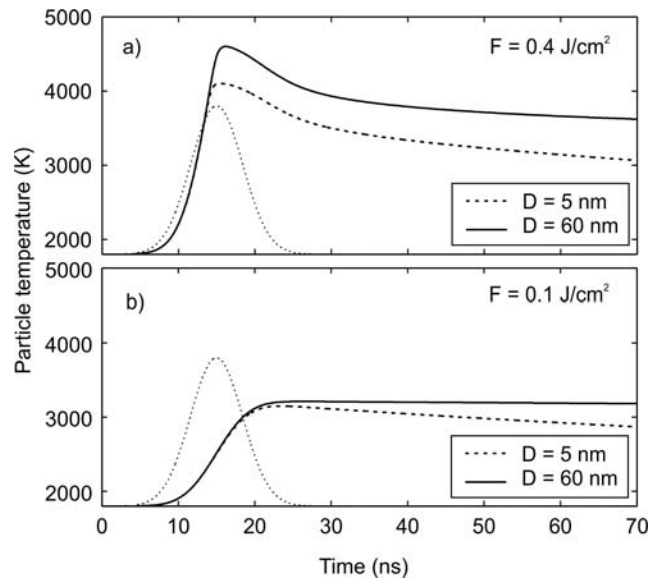
Figure 2. Theoretically calculated particle temperatures for two primary particle sizes as function of time for ambient gas temperature and pressure 1800 K and 0.1 MPa respectively. a) shows the results from using a high laser fluence and b) shows low-fluence results. The temporal distribution of the laser pulse is indicated.
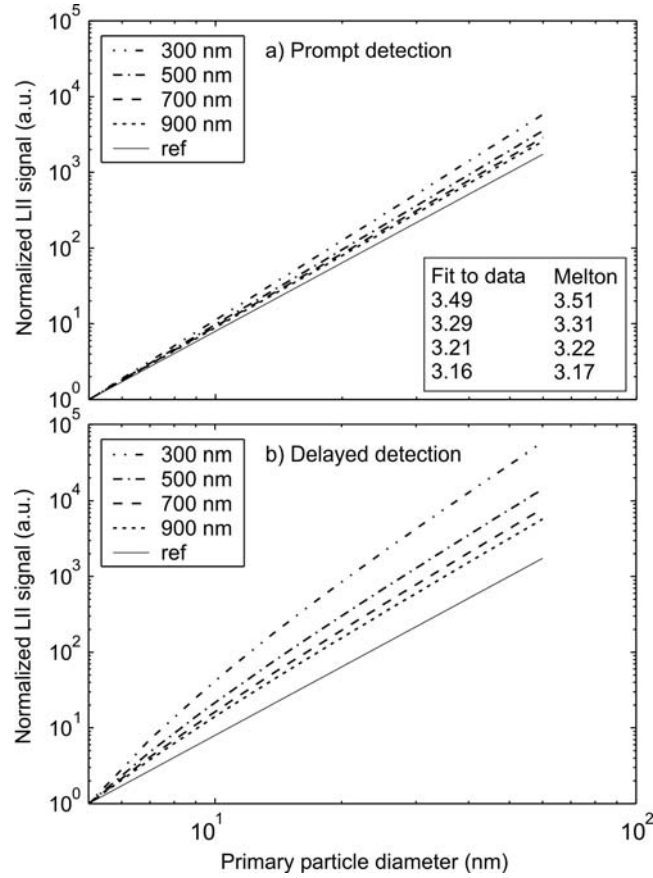
Figure 3. Prompt LII signal vs. primary particle diameter for different detection wavelengths (single-wavelength detection) and high fluence (0.4 J/cm^2). In a) the results obtained using a 20 ns prompt gate are shown whereas the results in b) show the case where the 20 ns gate is delayed 100 ns with respect to the case in a). The exponent x of a power law has been derived for a) using a power fit to the model data, and by using the Melton expression given in Eq. 2. Also shown are references lines corresponding the exponent x=3.
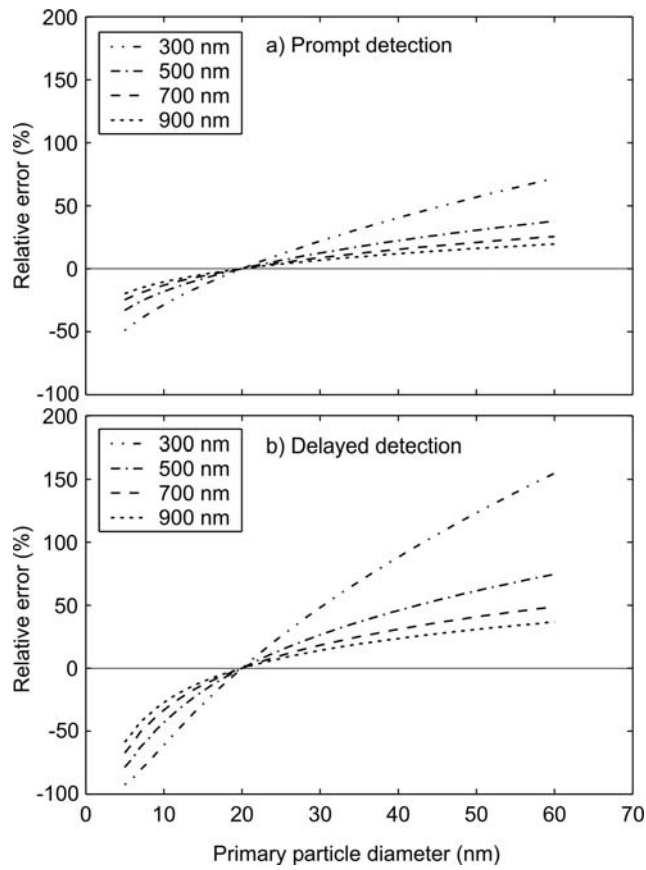
Figure 4. The relative error as function of detection wavelength for the base case at 0.4 J/cm^2. In a) the error is shown for a prompt 20 ns gate and in b) for a 20 ns gate delayed 100 ns with respect to the case in a). Note that this figure shows the same case as Fig. 3 but using another representation.
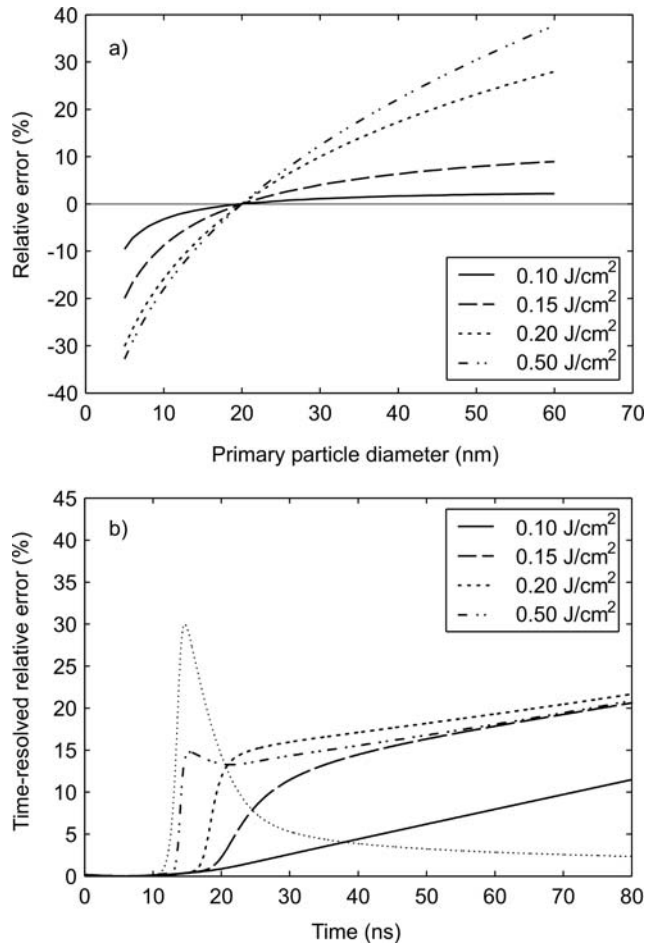
Figure 5. The relative error as function of laser fluence for the base case. In a) the error is shown for the case of gated detection (20 ns, prompt) and in b) the time-resolved error obtained for a particle with a size of 30 nm relative to the reference particle size of 20 nm is shown. Also shown is the LII signal for 30 nm particles at 0.5 J/cm^{2} (dotted line).
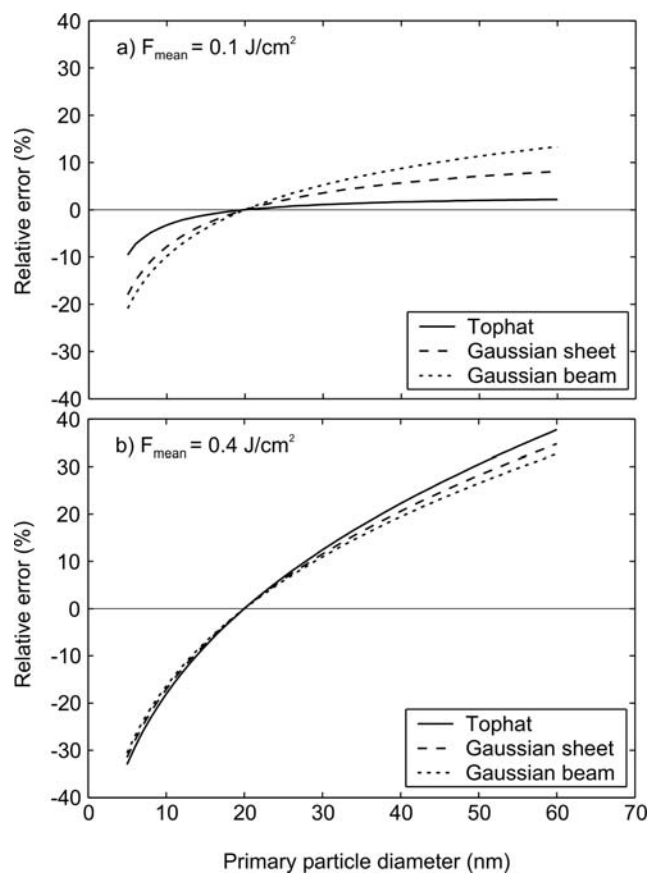
Figure 6. The relative error as function of the spatial profile of the laser beam when using gated detection (20 ns prompt). The three compared cases have the same mean laser fluence, which in (a) is 0.1 J/cm^2 and in (b) 0.4 J/cm^2.
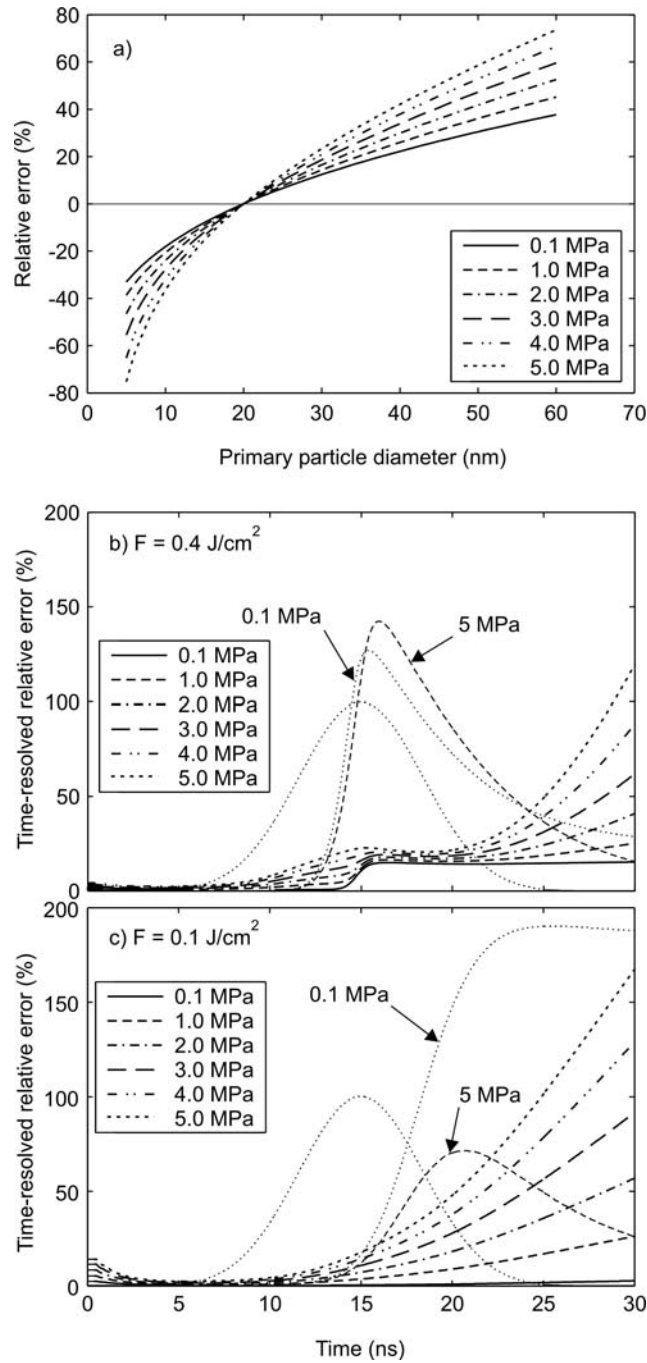
Figure 7. The relative error as function of gas pressure for the base case. In a) the relative error for gated detection (20 ns prompt) and a laser fluence at 0.4 J/cm² is shown whereas b) and c) shows the time-resolved error obtained at 30 nm with respect to a reference size of 20 nm for 0.4 J/cm² and 0.1 J/cm² respectively. The dotted bell-shaped curve marks the laser pulse. Also indicated are the predicted LII signals for the lowest and highest pressure for a particle size of 30 nm. Both LII signals in a figure have been scaled by the same value enabling relative signal comparison.
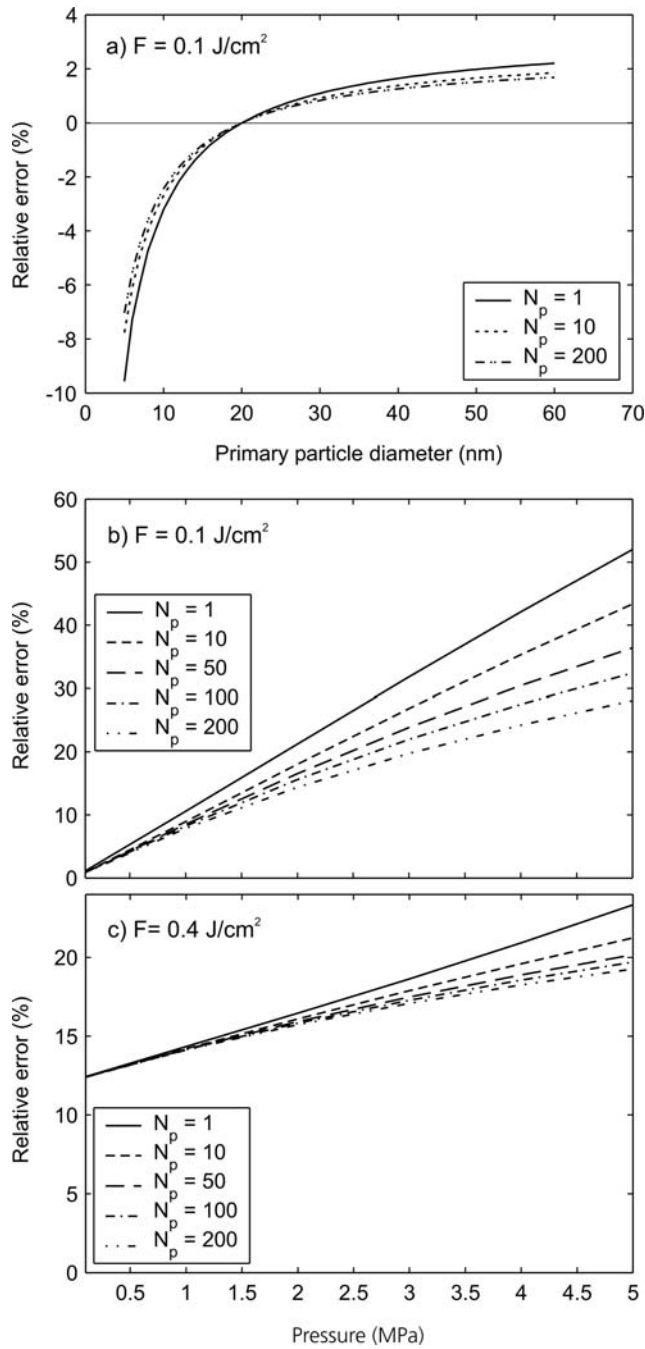
Figure 8. The relative error as function of the level of aggregation. In a) the relative error is shown for the base case at low fluence (0.1 J/cm^2) for different number of primary particles per aggregate, N_p. In b) and c) the relative error obtained at a particle size of 30 nm with respect to a reference size of 20 nm is shown for (b) low fluence and (c) high fluence as function of pressure and for different number of primary particles per aggregate.
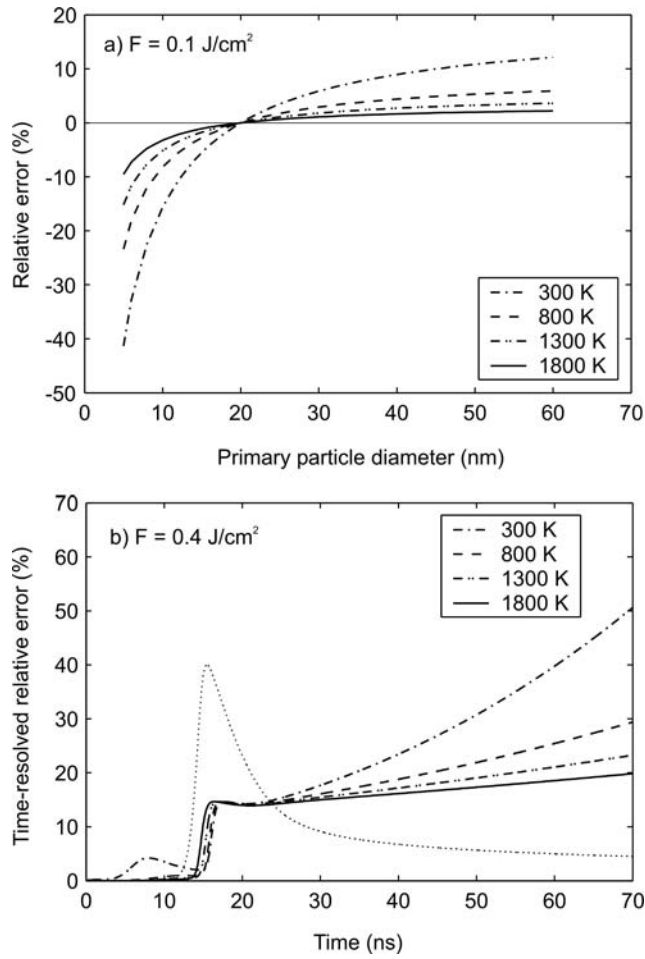
Figure 9. Influence of the gas temperature on the relative error. In a) the error for the base case is shown using gated detection (prompt 20 ns) at 0.1 J/cm^2 and in b) the time-resolved error obtained at a particle size of 30 nm with respect to a reference size at 20 nm is shown for varying gas temperature and a fluence of 0.4 J/cm^2. Also shown is the LII signal for 30 nm particles at 1800 K. The reported laser fluence values are for the 1800 K case only. The laser fluence for the lower gas temperatures has been increased in order to attain the same maximum particle temperature for all compared gas temperatures at a given value of the primary particle diameter.
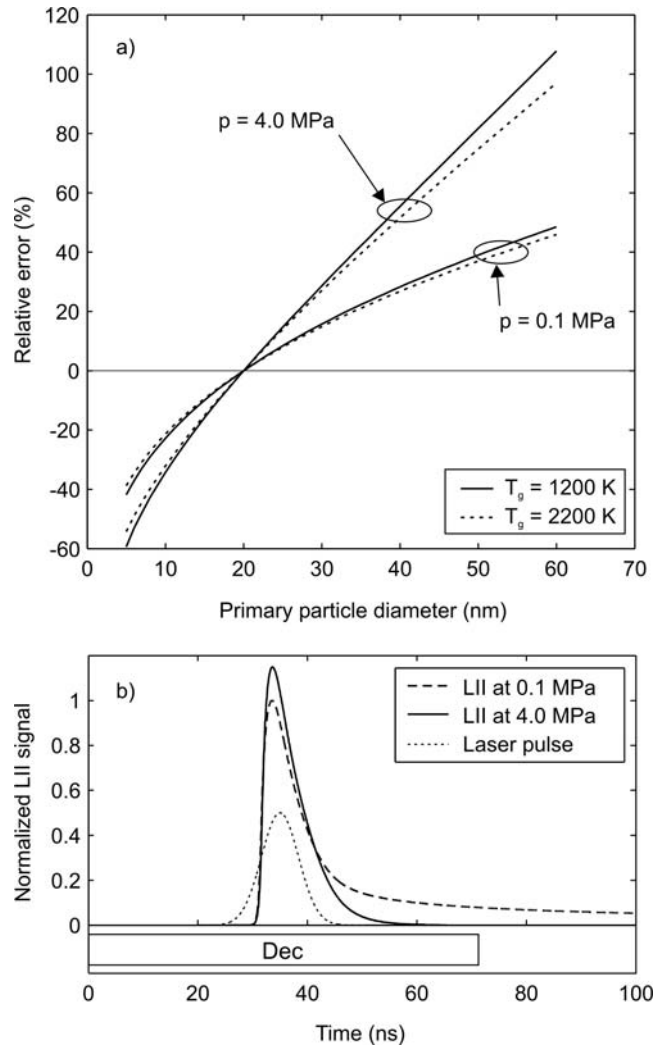
Figure 10. Results for the experimental approach by Dec [29] using the parameters in Table 2. In a) the relative error estimated for two different pressures and temperatures is shown as function of primary particle diameter, and in b) the modelled LII signals at 30 nm and T_g = 1200 K is shown together with the temporal distribution of the laser pulse. The LII signal at 0.1 MPa has been normalised, and the signal at 4.0 MPa has been proportionally scaled in order to keep the relative strengths between the two signals intact. The 70 ns gate used by Dec is indicated.
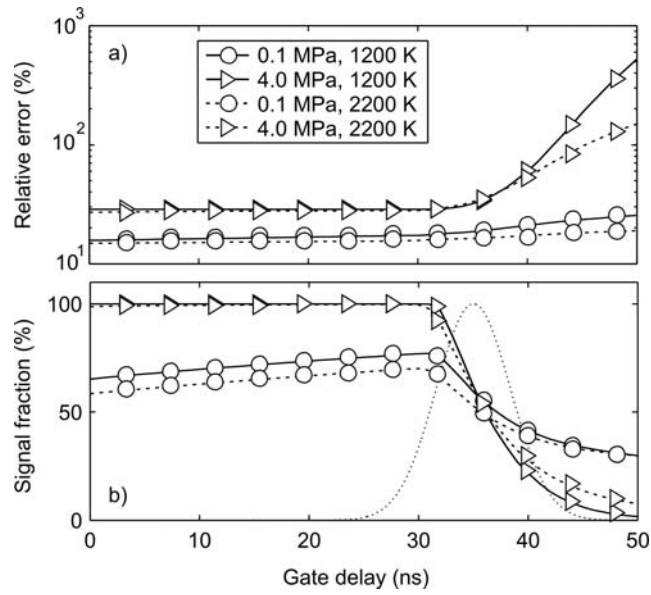
Figure 11. Predictions for the case described in Table 2 with varying delay time, defined relative to the default position of the gate (70 ns positioned centred on the laser pulse). In a) the relative error at the particle size 30 nm with respect to a reference size of 20 nm is shown for two different pressures and temperatures and b) the relative strength of the detected LII signal with respect to the total LII signal integrated between 0 and 300 ns is given. The position of the laser pulse is indicated (dotted line).
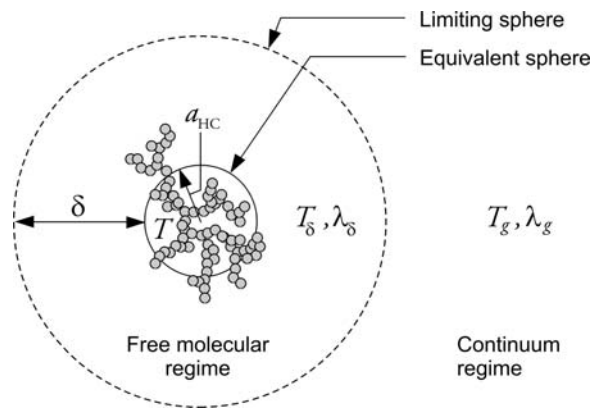
Figure A1. A schematic representation of the Fuchs heat conduction model applied for a soot aggregate using the equivalent sphere approach.

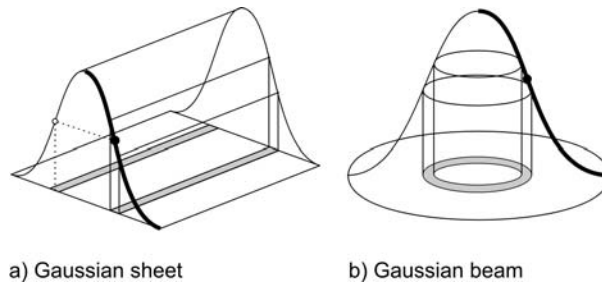a) Gaussian sheet   b) Gaussian beam

Figure A2. The two non-uniform spatial distributions of laser energy used within this study. The Gaussian function determining the fluence values, P^F, is indicated as thick lines together with the cross section areas determining the individual relative weights for the calculated LII signals.